An Investigation of Mixed Convection Flow on a Vertical Flat Plate of a Saturated Nanofluid in a Porous Medium near the Stagnation Point

Ali Shokrgozar Abbasi*
* *Assistant Professor, Department of mechanical engineering, Payame Noor University, Tehran, Iran*
(Corresponding Author, Tel. +989153131811, Email: shokrgozar.ali@pnu.ac.ir, *Tehran, Iran, P.O.Box. 19395-4697)*

Abstract:
In the present paper, a non-similar solution of a steady saturated nanofluid flow, heat, and mass transfer is investigated. The nanofluid flow is under dual effects of stagnation flow and natural convection heat transfer on a vertical flat plate in a porous medium. Effects of variations in thermophoresis, Brownian motion, and buoyancy force have been studied. The partial differential equations are transformed into six ordinary differential equations with appropriate non-similarity variables, which also consider the longitudinal coordinate of the x-axis. In order to solve, we have formed a set of fourteen ordinary differential equations of the first order. A complicated double method finds six unknown initial values in the boundary value problem. Variations of longitudinal velocity, shear stress, temperature, and nanoparticle volume fraction are considered as functions of transverse and longitudinal coordinates. As a result, the minimum accuracy of the first-order non-similar solution in regions very close to the stagnation point is 96%. Also, the velocity profile is observed to vary along the longitudinal x-axis near the stagnation point, which is an improvement over the existing knowledge which largely assumes a constant velocity profile throughout the stagnant flow region.

Keywords: Non-similar solution, dual effects, natural convection, stagnation flow, Nanofluid

Nomenclature

English	
a	Strain of the flow
C	Heat capacity coefficient
D_B	Brownian motion diffusion coefficient
D_T	Thermophoretic diffusion coefficient
g	acceleration of gravity
Gr_x	Grashof number
k	Thermal conductivity
K	permeability
p	pressure
N_B	Brownian motion parameter
N_T	Thermophoresis parameter
n	A constant
$\Pr$	Prandtl number $(=\frac{\nu}{\alpha})$
Re_x	Reynolds number $(=\frac{u\,x}{\nu})$
Sc	Schmidt number $(=\frac{\nu}{D_B})$
T	Temperature
U_∞	Far-field velocity
u,v	Velocity components in the x- and y-directions, respectively
x,y	Cartesian coordinates along the plate and normal to it
Greek	
β	Volumetric thermal coefficient
Γ	An empirical constant
σ_1,σ_2	Arbitrary coefficients
ε	Porosity
ξ,η	Nom-similar variables in the x-, y-directions, respectively
θ	Dimensionless temperature
λ	The mixed convection parameter, $\left(=\frac{Gr_x}{Re_x^2}\right)$
γ	A constant
ρ	Density

ν	kinematic viscosity
φ	nanoparticle volume fraction
ψ	Stream function
Δ_1, Δ_2	Dimensionless resistance of permeability, first and second order, respectively, $\left(=\frac{\nu}{a}\frac{1}{K}, =\Gamma\sqrt{\Delta_1}\right)$
Subscript	
c, T	Concentration and thermal expansions, respectively
p, f	Nanoparticle and base fluid, respectively
w, ∞	Conditions at wall and infinity, respectively
Superscript	
$'$	Differentiation with respect to $\xi(for\ F, R, S)$ or $\eta(for\ f, \theta, \varphi)$

1. Introduction:

Heat transfer is key to several industrial processes encompassing solar thermal applications, nuclear power generation, electronic equipment cooling, manufacture of chemical feedstocks, as well as a wide array of state-of-the art sensitive installations custom-made for the military establishments. The use of various types of solar thermal collectors is accompanied by optical, thermal, and thermodynamic analysis to evaluate their performance. Some of these applications constitute thermal treatment in integrated collector storage, direct and indirect air systems, space heating and cooling, refrigeration, and heat transfer in industrial processes [1]. Since the major energy losses from solar systems constitute convective heat transfer, radiation emission and reflection, heat transfer analysis are essential for the design and optimization of solar thermal energy systems for electricity generation, chemical fuel production and energy processing [2]. The main focus, in the field of nuclear power generation revolves around ensuring safety. This involves analyzing blueprints and obtaining authorization for nuclear power plants all while considering safety assessments carried out through dedicated computational codes that deal with heat and mass transfer. Additionally due to the fission reactions or residual heat within the core of a nuclear power plant specialized thermal exchange systems are necessary to dissipate heat and manage mass. These systems play a role in designing nuclear systems [3]. A significant issue in heat transfer with advances in micro- and nano-fabrication capabilities has been heat removal in devices such as computer chips, laser diodes, and electronic components [4]. Heat management issues are facing critical challenges with rapid increase in heat flux and continuous miniaturization of electronic devices. Common electronic cooling methods are classified into direct and indirect methods, direct cooling includes jet impingement and spray cooling, air cooling, droplet humidification and immersion cooling. The most popular methos of indirect cooling are the use of thermoelectric, microchannel, vapor chamber, heat pipe and "Pulse Code Modulation (PCM)" [5].

First, we discuss the stagnation flow and heat transfer and solution methods. In general situations, the flow in a stagnation point region is only dependent on transverse y-coordinates, so the similarity solution method is the most common in stagnation flow research. since the method facilitates ease of implementation and is devoid of any major computational overhead. Weidman and Mahalingam [6] investigated the flow and heat transfer in a stagnation flow, at the same time, the fluid is viscous, and its coordinates have damped oscillatory motion. Temperature profiles, velocity profiles, and stress tensors in stagnation flow for different values of Prandtl numbers and velocity ratios are presented for different transpiration of the flat plate [7]. In the case of bounding the flow pattern from both sides, non-axisymmetric stagnation flow may occur in the presence of any physical limitation [8]. In two-dimensional and cylindrical unsteady stagnation flow, while the substrate plate moves towards the flow, the effect of the plate velocity variations on the thickness of velocity and thermal boundary layers is more than that of the acceleration, so maximum plate velocity produces minimum boundary layer thickness. Its acceleration effect plays a secondary role [9, 10]. Heat transfer and fluid freezing in stagnation flow are the most significant natural phenomena and have many industrial applications. Stephen's solidification problem for viscous fluid in stagnation flow is solved by Rangel and Bian [11]. Investigating the freezing of the incompressible fluid in Cartesian two-dimensional and three-dimensional axisymmetric stagnation flow shows that Stephen number is ineffective in the final ice thickness. However, it is effective in freezing time, and by increasing the Prandel number by ten times, the final thickness of the ice is approximately halved. Also, when the process reaches steady-state condition, there is a significant difference between the thickness of the ice in the Cartesian two-dimensional and axisymmetric three-dimensional coordinate systems [12, 13]. In calculating air vapor freezing theory in a two-dimensional stagnation flow, the cell size next to the substrate plate controls the onset time of condensation, contrary to physical experiments. Here, it was found that the maximum time before freezing begins for the size of both 0.1 and 0.2 mm are the same, at about the 5℃ air temperature [14]. Yih [15] also studied the heat effect in two-dimensional flow under Magnetohydrodynamics convective heat transfer in

stagnant flow. In his numerical study, the plate was permeable, and its heat was assumed to be linear. He used a Keller box method to solve the problem and concluded that the auxiliary (opposite) buoyancy force increases (decreases) the local Nusselt number and the local friction coefficient. Also, he showed that the local Nusselt number is nearly constant for very small or significant permeability.

Adding nanoparticles to the fluid increases the heat transfer. Recently, research on the effect of nanofluid on heat transfer enhancement has expanded. The multiplicity of applications has caused great diversity in the field of research; even, the research methods are very diverse. Heat transfer with ultrahigh-performance is one of the vital needs of many industrial technologies. Whereas, inherently low thermal conductivity is a primary limitation in development energy-efficient heat transfer fluids. Nanofluids with their enormous potential provide enhanced ultrahigh-performance heat transfer. Innovative engineering efforts have shown that incorporating amounts (less than 1% by volume) of nanoparticles into host fluids can greatly enhance their thermal properties. For instance certain nanofluids exhibit characteristics such as increased thermal conductivity at low nanoparticle concentrations, thermal conductivity that depends heavily on temperature and particle size a non linear relationship between thermal conductivity and concentration and a notable threefold increase in critical heat flux at an extremely low particle concentration of around 10 parts, per million (ppm) [16]. Note that a nanoparticle suspension is considered as a triple phase system including the fluid media (liquid phase), the nanoparticles (solid phase), and the interfacial phase, which significantly affects the properties of the system due to the extremely high surface area of nanofluid relative to its volume [17]. Another significant research area in fluid dynamics is the thermal performance for unsteady boundary layer flow of nanofluids in the presence of suction/injection. This flow situation is broadly used in space sciences and aerodynamics as well [18]. Enhanced thermophysical properties of nanofluids is the primely reason for increasing attention. These properties include their ability to contribute into a wide range of thermal applications ranging from harvesting solar energy to produce renewable energy to increasing the efficiency of heat exchangers used in industrial [19]. So, Nanofluids are attracting a great deal of interest with respect to particularly their heat transfer properties.

Now we follow the discussion of mixed convective flow with or without nanofluid in the presence or absence of a porous medium when the velocity of the fluid in contact with the plate is low enough and the plate is hot. In the direction of gravity acceleration, the effects of stagnation flow and natural convection cause the fluid to move. Cheng [20] investigated the problem of free and forced hybrid convection on wedges in a saturated porous medium. He found that Gr/Re is a parameter governing the mixed convection on the wedges in the porous medium. His research focused on two modes of constant temperature and constant heat transfer of the sloping plate, and the temperature and velocity profiles for different values of Gr/Re were presented. As the value of Gr/Re approaches the limits of infinity and zero, it has been shown to aid the flows that the heat transfer velocity is asymptotically close to the free or forced convection values. Nazar et al. [21] considered a vertical flat plate in a porous medium. They investigated the flow of the convective boundary layer in the stagnation flow of a saturated nanofluid. In their study, the flow instability was due to the formation of impulsive motion and a sudden increase in plate temperature. They showed that we have solutions for a limited range λ, for opposing flow $(\lambda<0)$ or assisting flow $(\lambda>0)$, where λ is the mixed convection parameter. Following the previous study, Merrill et al. [22] used numerical evidence to find the second solution for $\lambda>-1$. They also prove that if $\lambda<-2.9136$ for the boundary value problem, there is no solution. Also, in the continuation of the research, Ishaq et al. [23] proved that there are dual solutions with opposite flows for the assisting flow. Subhashini et al. [24] developed a mixed convection nanofluids flow near the stagnation point region over an exponentially shrinking/stretching sheet using the local similarity method.

If the flow also depends on the longitudinal x-coordinates, another solution method can be used to solve the problem, such as the non-similar solution method. Note that the non-similar solution method is suitable for the small variations in a second independent variable, such as the variations in the longitudinal x-coordinates studied in the work.

Notice, in the case of suction/blowing, or if the heat transfer rate depends on the longitudinal x-coordinate, the effects of the longitudinal x-coordinate must be taken into account [25]. More precisely, if the lateral mass flux has temperature variations as $T_w = T_\infty + Ax^\gamma$, and the suction/blowing velocity is given by $v_w \sim ax^n$, then the similarity solutions are admitted, if $n=\frac{(\gamma-1)}{2}$.(where the plate's temperature, the far-field temperature, and the coordinate along the plane are T_w ,T_∞, and x , respectively.) [26, 27]. Therefore, in general, in the case of suction/blowing, or if the temperature of the lateral mass flux depends on the longitudinal coordinates x along the bed surface, the accuracy of the similarity solution should be evaluated, or a non-similar method should be used to solve the problem. Jafarimoghaddam [28] has focused on a permeable

linearly stretching/shrinking wall in stagnation flow immersed in nanofluids. He has concluded that the influence of important parameters in classical nanofluid modeling is ambiguous. He also has found that the lower branch of dual solutions (for example, up and down) is not supposed to be in actual physics. Roşca et al. [29] have investigated a steady mixed convection stagnation flow of a hybrid nanofluid. They have also applied the similarity solution method using second-order slip velocity. Ferdows et al. [30] have investigated the steady two-dimensional free convection flow of a saturated nanofluid on a flat plate in a porous medium, where the flow is laminar and incompressible. Also, the effects of thermal and mass transfer have been considered in their study. They also have solved the problem using the similarity solution method. They have presented the effects of the pertinent dimensionless parameters on the problem. Prasad et al. [31] have presented a similar solution of the laminar mixed convection flow around a heated surface in a two-dimensional stagnation point region. Duwairi et al. [32] have used a numerical solution to investigate the effects of the oscillating plate temperature on the transient mixed convection heat transfer of a porous medium saturated by a vertical porous surface. Ishake et al. [33] have presented a similar solution of the flow through a porous medium bounded by a vertical surface in the steady stagnation point. Srinivasacharya and Surender [34] have studied the effects of thermal and mass stratification on the flow of the natural convection boundary layer on a vertical plate embedded in a porous medium saturated with a nanofluid. Abdullah et al. [35] have studied the non-similar solution of unsteady convection nanofluid mixing of a hot vertical plane in stagnant flow, in which time is chosen as the non-similar variable. Therefore, the changes in the longitudinal axis are not taken into account. However, when the temperature depends on the longitudinal coordinate x-axis, the x-axis should be selected as the non-similar variable. Ferdows and Alzahrani [36] have investigated a steady two-dimensional free convective flow of a nanofluid on a flat plate saturated in a porous medium, where the flow is laminar and incompressible. The effects of thermal and mass convection are taken into account in their study. They also solved the problem using the similarity solution method and presented the effects of the pertinent dimensionless parameters on the problem. Waini et al. [37] have investigated a stagnation hybrid nanofluid flow on a stretching/shrinking cylinder. They used the similarity solution to find the increase in heat transfer rate and skin friction coefficients in the presence of nanofluid. Recently, Khan et al. [38] have considered a convective stagnation flow mixed with the presence of radiation on a yawed cylinder. Their solution method was the non-similar and used nanofluid as the working fluid. They have shown the effect of volume fraction of hybrid nanoparticles, mixed convection, and radiation in their research. Note that a Nusselt number for mixed convection gives a higher heat transfer coefficient than the forced convection in a specified range of Rayleigh and Reynolds numbers, which is one of the advantages of combined convection [39].

Rashad et al. [40] have investigated mixed convection flow micropolar nanofluid. They have considered the opposing and assisting convective flows of Titania and Alumina nanoparticles by a non-similar solution using the Rung-Kutta method. They have shown that Biot number, material properties, mixed convection, and nanoparticle volume fraction affect heat transfer. However, they have not used the longitudinal x-axis as the secondary non-similar variable. Hossein et al. [41] have considered mixed convection of a CuO-water nanofluid in a trapezoidal enclosure, and a rotating cylinder in the enclosure with special boundary conditions in which the lower space of the enclosure has a porous medium. They have found that increasing the volume fraction, Rayleigh and Darcy numbers, the angular velocity of the cylinder and the inner radius increases the average Nusselt number. Among the applications of this method in the solution of heat or mass transfer problems are a two-dimensional G-jitter hybrid convective flow of a nanofluid by Uddin et al. [42], and Magnetohydrodynamics transport of a non-Newtonian nanofluid on a circular cylinder by Prasad et al. [43]. Another research on nanofluid, in an enclosure of mixed convective heat transfer has been done by Farhani and Abdulsaheb [44]; however, they have considered a square enclosure with Al2O3–water nanofluid and have used Galerkin finite element method. Increasing the value of Rayleigh number, Darcy number, and solid volume fractions increase the average Nusselt Number, flow, and temperature gradient intensity. Recently, Nabwey et al.[45] considered a mixed convection flow nanofluid containing gyrotactic microorganisms with effects of Suction/injection by using a mathematical model on a vertical surface in a porous medium. They have shown that increasing the Peclet number increases the motile microorganism number. Also, the growth of the thermophoresis parameter provides conditions for injection, where the opposite behavior occurs in the case of suction.

In this article, we are concerned about the mixed convection heat transfer and fluid flow of a nanofluid in a saturated porous medium in a stagnation point region. At the same time, the longitudinal coordinate (the x-axis) effects are considered. In the previous publications that use the non-similarity solution method, the secondary non-similar variable is not the longitudinal x-axis; accordingly, the variations of the parameters on the longitudinal x-axis are ignored, but is this

assumption valid? In the present paper, we consider the reality of the assumption. Non-similar solution method is obtained to solve the governing equations, with longitudinal coordinate x-axis as the secondary non-similar variable. The effects of thermophoresis motion, Brownian motion, buoyancy force, more importantly, the effects of variations along the x-axis of longitudinal coordinate have been investigated. Again, in general, it is essential to note that in the presence of suction/blowing, or if the lateral mass flux temperature depends on the x-coordinates along with the substrate plate, the similarity solution method lacks the necessary precision and is not admitted.

2. Problem Statement and Formulation:

A schematic representation of the problem is shown in Figure 1. A horizontal fluid flow vertically moves towards a semi-infinite flat plate embedded (immersed) in a saturated porous medium. The mixed convection flow is dominant because the buoyancy force is not negligible. In the equilibrium state, consider that the plate surface is maintained at a constant nanoparticle fraction ϕ_w and constant temperature T_w. In contrast, the upper section of the y-axis is in T_{wh}, and the lower section is in T_{wc}. The nanoparticle fraction and temperature in the far-field are ϕ_∞ and T_∞, respectively. The buoyancy effect assists the upper and the lower sections of the flow because T_{wh} is higher thanT_∞, and T_{wc} is low.

Notice that the problem is solved only in the buoyancy assisting regions (the heated region in Fig.1).

In these conditions, the governing equations, including the conservation of mass, momentum, variations of pressure, energy, and nanoparticle volume fraction, for steady mixed convection, can be expressed as follows, respectively:

$$\frac{\partial u}{\partial x}+\frac{\partial v}{\partial y}=0 \tag{1}$$

$$\frac{1}{\varepsilon}\left(u\frac{\partial u}{\partial x}+v\frac{\partial u}{\partial y}\right)=-\frac{1}{\rho_f}\frac{\partial p}{\partial x}+\nu\frac{\partial^2 u}{\partial y^2}-\frac{\nu}{K}u$$
$$-\frac{\Gamma}{\sqrt{K}}u^2+\left[\beta_T\left(1-\phi_\infty\right)\left(T-T_\infty\right)-\left(\phi-\phi_\infty\right)\left(\frac{\rho_P}{\rho_f}-1\right)\right]g \tag{2}$$

$$-\frac{1}{\rho_f}\frac{\partial p}{\partial x}=\frac{U_\infty}{\varepsilon}\frac{\partial U_\infty}{\partial x}+\frac{\nu}{K}U_\infty+\frac{\Gamma}{\sqrt{K}}U_\infty^{\,2} \tag{3}$$

$$u\frac{\partial T}{\partial x}+v\frac{\partial T}{\partial y}=\alpha_m\frac{\partial^2 T}{\partial y^2}$$
$$+\varepsilon\frac{\left(\rho C\right)_P}{\left(\rho C\right)_f}\left[D_B\frac{\partial T}{\partial y}\frac{\partial \phi}{\partial y}+\frac{D_T}{T_\infty}\left(\frac{\partial T}{\partial y}\right)^2\right] \tag{4}$$

$$u\frac{\partial \phi}{\partial x}+v\frac{\partial \phi}{\partial y}=\varepsilon D_B\frac{\partial^2 \phi}{\partial y^2}+\varepsilon\frac{D_T}{T_\infty}\left(\frac{\partial^2 T}{\partial y^2}\right) \tag{5}$$

where ε is porosity, K is permeability, Γ is empirical constant, β_T is the volumetric thermal coefficient, D_T and D_B are Thermophoresis and Brownian diffusion coefficients, respectively. A variety of potential pressures are also expressed in Eq. 3. Equation 4 is obtained by assuming that the pressure changes along the thickness of the viscous layer are negligible. Based on this, the pressure changes inside the viscous layer can be considered only along the longitudinal axis. The Bernoulli equation can be used for pressure variations outside the viscous layer.

Also, boundary conditions can be expressed as follows:

$$u_{y=0}=0,\qquad u_{y\to\infty}=U_\infty=a\,x$$
$$v_{y=0}=0,\quad T_{y=0}=T_w,\quad \phi_{y=0}=\phi_w \tag{6}$$

Equations can be transported to two non-dimensional coordinate systems by appropriate non-similarity variables,

$$\xi=x\sqrt{\frac{a}{\nu}}\ ,\ \eta=y\sqrt{\frac{a}{\nu\xi}} \tag{7}$$

Where ξ,η [23] are the non-dimensional variables in the directions of the x and y-axis, respectively, a is the strain, and ν is the viscosity of the fluid. The velocities in the directions ξ and η in the new coordinate system can be shown by the function ψ and the above non-similar variables as follows, which satisfy the continuity equation:

$$u=\sqrt{a\nu}\,\xi f\,'_{(\xi,\eta)}$$
$$\psi=\nu\int\xi^{3/2}f\,'d\eta$$
$$v=-\sqrt{a\nu}\left(\xi^{1/2}f+\xi^{3/2}\frac{\partial f}{\partial \xi}\right) \tag{8}$$

Where $f=f\left(\xi,\eta\right)$ and the derivative relative to η is displayed with ('). Non-dimensional temperature and nanoparticle volume fraction also can be expressed as below:

$$\theta(\xi,\eta)=\frac{T-T_\infty}{T_w-T_\infty},\quad \varphi(\xi,\eta)=\frac{\phi-\phi_\infty}{\phi_w-\phi_\infty} \tag{9}$$

Equations 2,4 and 5 are transformed by using 7-10 in equations:

$$\begin{aligned} f'''=&-\frac{\xi}{\varepsilon}\left(1-f'^2+ff''\right)-\Delta_1\xi\left(1-f'\right)-\sigma_2\varphi\\ &-\Delta_2\xi^2\left(1-f'^2\right)-\xi\lambda\theta+\frac{\xi^2}{\varepsilon}\left(f'F'-f''F\right)-2F' \end{aligned} \tag{10}$$

$$\theta''=-\xi\,\mathrm{Pr}\,f\,\theta'-\mathrm{Pr}\,N_B\,\theta'\varphi'-\mathrm{Pr}\,N_T\,\theta'^2+\mathrm{Pr}\,\xi^2\left(f'R-\theta'F\right) \tag{11}$$

$$\varphi''=-\frac{\mathrm{Sc}}{\varepsilon}\xi f\,\varphi'-\frac{N_T}{N_B}\theta''+\frac{\mathrm{Sc}}{\varepsilon}\xi^2\left(f'S-\varphi'F\right) \tag{12}$$

Where $\mathrm{Pr}=\frac{\nu}{\alpha}$, $Sc=\frac{\nu}{D_B}$ are the Prandtl and Schmidt Numbers, respectively $(\mathrm{Pr}=Sc=10)$ and other parameters are presented in the following table:

$\Delta_1=\frac{\nu}{a}\frac{1}{K}$	first order dimensionless, resistance of permeability
$\Delta_2=\Gamma\sqrt{\Delta_1}$	second order dimensionless, resistance of permeability
$\sigma_1=\frac{(\rho C)_P}{(\rho C)_f}$	An arbitrary coefficients
$\sigma_2=\frac{g}{a\sqrt{a\nu}}\times\left(1-\frac{\rho_P}{\rho_f}\right)(\phi_w-\phi_\infty)$	An arbitrary coefficients
$N_{T1}=\frac{D_T}{\nu}\frac{T_w-T_\infty}{T_\infty}$ $N_T=\varepsilon\sigma_1 N_{T1}$	N_T: Thermophoresis parameter
$N_{B1}=\frac{D_B}{\nu}(\phi_w-\phi_\infty)$ $N_B=\varepsilon\sigma_1 N_{B1}$	N_B: Brownian motion parameter
$\lambda=\frac{Gr_x}{Re_x^2}=\frac{g\beta(T-T_\infty)}{a^2x}$	The mixed convection parameter

Due to the close weak correlation between the x dimension and the temperature, the similarity solution has an error [14], so the non-similarity solution is used in the present paper. For this purpose, the derivatives of the functions f,θ,ϕ for ξ are called *F, R, S*, respectively:

$$F=\frac{\partial f}{\partial\xi},\quad R=\frac{\partial\theta}{\partial\xi},\quad S=\frac{\partial\varphi}{\partial\xi} \tag{13}$$

The equation obtained from the derivative of equations 10 to 12 with respect to ξ is the effect of the longitudinal dimension of that equation. Here, second-order derivatives relative to ξ are omitted due to their small size:

$$\begin{aligned} F'''=&-\frac{1}{\varepsilon}\left(1-f'^2+ff''\right)-\Delta_1\left(1-f'-\xi F'\right)\\ &-\frac{\xi}{\varepsilon}\left(-4f'F'+3Ff''+fF''-\xi F'^2+\xi F''F\right)\\ &-2\Delta_2\xi\left(1-f'^2-\xi f'F'\right)-\sigma_2 S-\lambda\left(\theta+\xi R\right) \end{aligned} \tag{14}$$

$$\begin{aligned} R''=&-\mathrm{Pr}f\,\theta'-\mathrm{Pr}\xi F\theta'-\mathrm{Pr}\xi fR'\\ &-\mathrm{Pr}N_B\left(R'\varphi'+\theta'S'\right)-2\mathrm{Pr}N_T\theta'R'\\ &+\mathrm{Pr}\xi\left[2f'R-2\theta'F+\xi F'R-\xi R'F\right] \end{aligned} \tag{15}$$

$$\begin{aligned} S''=&-\frac{\mathrm{Sc}}{\varepsilon}\left(f\,\varphi'+\xi F\varphi'+\xi fS'\right)-\frac{N_T}{N_B}R''\\ &+\frac{\mathrm{Sc}}{\varepsilon}\xi\left[2f'S-2\varphi'F+\xi F'S-\xi S'F\right] \end{aligned} \tag{16}$$

The boundary conditions for solving the above differential equation system are:

$$\begin{aligned} &f_{\eta=0}=0,\ f'_{\eta=0}=0,\quad f'_{\eta\to\infty}=1\\ &\theta_{\eta=0}=1,\quad \theta_{\eta\to\infty}=0\\ &\varphi_{\eta=0}=1,\quad \varphi_{\eta\to\infty}=0 \end{aligned} \tag{17}$$

$$\begin{aligned} &F_{\eta=0}=0,\ F'_{\eta=0}=0,\quad F'_{\eta\to\infty}=1\\ &R_{\eta=0}=1,\quad R_{\eta\to\infty}=0\\ &S_{\eta=0}=1,\quad S_{\eta\to\infty}=0 \end{aligned} \tag{18}$$

Here, six boundary conditions at the beginning of the boundary are unknown, so we have to use the shooting method $(f''_{\eta=0},\ \theta'_{\eta=0},\ \varphi'_{\eta=0},\ F''_{\eta=0},\ R'_{\eta=0},\ S'_{\eta=0})$.

3. Numerical Solution Method:

We use the 45 Runge–Kutta method with the shooting approach to solving the ordinary differential equations. In this method, first, the answer is obtained with two accuracies of fourth and fifth order, and they are compared with each other. If the accuracy of these two is more than the desired accuracy, the answer is accepted. Otherwise, the mesh sizes become smaller, and this operation continues until the desired accuracy is achieved. Fourteen first-order differential equations with six initial guesses must be solved simultaneously to obtain the answers. We have chosen the minimum accuracy of the answers to be 0.00001. Note that the above equations are nonlinear, and therefore, the initial guess for finding the answer faces certain complexities. Since forming Jacobin equations which based on Newton's method is first-order accuracy, finding the initial guess by this method has minimal application, so it has only been used to increase the accuracy from 0.001 onwards. Remember that Runge-Kutta-Fehlberg Method (or RKF45) is a method of order O(h4) with an error estimator of order O(h5).

The prepared code in this article is very complex and uses several consecutive methods to find the answers. First, by removing equations 14 to 16 and non-similar variables, the answers to the similarity problem are obtained. The answers are the initial guesses for the primary problem. It is clear that in this case, we get the answers much faster. Then, at each step, by adding a minimal amount of non-similar effects and their equations, for example, 1%, we gradually approach the solutions of the non-similar problem. The code automatically increases the convergence step by at least 0.001. Then the accuracy of the answers increases to 0.00001 by forming Jacobin equations based on Newton's method. Also, the code intelligently detects inverse changes leading to divergent answers and corrects them with appropriate changes.

4. Validation:

We have compared between similarity and non-similarity solutions for validation. In general, the solution of similarity and non-similarity will not have the same answers to this problem when the temperature has a variable value relative to ξ-axis; We are only allowed to use the solution of non-similarity; however, the similarity solution is acceptable only for particular points of the longitudinal axis. We have used these particular points for validation and, even more importantly, for the accuracy of the non-similarity solution.

In Figure (2), we show the similarity and non-similarity solutions of the changes f', which represent the velocity variations in the x-direction, for the case where θ and ϕ have a constant value on the longitudinal axis ξ, $\theta_{wall}, \phi_{wall} = 1$. As can be seen, with a point close to the stagnation point, ξ = 0, the difference between the two similarity and non-similarity solutions increases. The non-similarity solution graph of ξ = 1 approximately matches the similarity solution one, and the error is less than 2%, which indicates the maximum error of the non-similarity solution. Note that the error is due to a difference between the derivatives relative to ξ and the zero in the momentum equation (Eq. 14) at ξ=1. Furthermore, the maximum difference between the answers to the non-similarity solution at the points ξ=0.25 and ξ=1 is about 9%, so the maximum non-similarity error between points close to the point of stagnation and far away from it cannot be more than 7%. Also, since the more the non-similarity diagrams coincide with the tendency towards ξ=1, we conclude that expansion with a first-order approximation is suitable for these points. It can be concluded that the first-order expansion ξ=0.5 and more is specific accurate enough. In contrast, with a further decrease in ξ, for higher accuracy, higher-order expansion may be required, which is beyond the scope of this paper.

In Figure 3, we show the similarity and non-similarity solutions of the f' curve in the case of $\theta = \phi = \xi^n$, n = 1. Interestingly, the f' profile answers of the non-similarity solution are much closer to that of the similarity solution in the previous case, where the values of θ and ϕ were constant on the longitudinal axis ξ; So the profiles for $\xi \geq 0.5$ are almost the same. The maximum difference between the two curves is less than 4%. Note that part of the 4% error is due to first-order expansion in problem-solving. Also, if ξ was not explicitly present in the equations, we were allowed to use the similarity solution, which means that the similarity solution had to be answered with sufficient accuracy [18]. Again, if the lateral mass flux has temperature variations as $T_w = T_\infty + Ax^\gamma$, and the suction/blowing velocity is given by $v_w \sim a x^n$, then the similarity solutions are admitted, if $n = \frac{(\gamma - 1)}{2}$ [17,18]. Here, the validation of temperature equations is done the same way that the validation of motion equations.

Temperature profile changes for constant wall temperature $\theta_{wall} = Constant$ are shown in Figure 4. According to what was seen in Figure 2, the difference between similarity and non-similarity diagrams is expected to be significant in small ξ. Gradually approaching ξ = 1, this difference is minimized, which can be seen in Figure 4.

Here, since the temperature changes follow the equation $\theta_{wall} = \xi$, we expect to have to use the non-similarity solution [17]. As shown in Figure 5, the similarity and non-similarity curves at ξ = 0.75,1 have been matched with reasonable accuracy, more than 99%, which indicates the accuracy of the

similarity solution at points far from the point of stagnation in heat transfer.

5. Results and Discussion

In this section, we present the results and discuss them. Here, the effect of the Brownian motion, thermophoresis motion, buoyancy force, and the effect of the study point position along the longitudinal x-axis, which is assumed to be negligible in the similarity solution are investigated. First, complete problem-solving results are provided for all unknown variables (Figures 6 and 7):

As can be seen in Figure 7, the velocity derivative respect to x (or ξ) in the direction of the η-axis tends to have a unique value. The unique value is proportional to potential velocity. Derivatives of other variables tend to be zero relative to x .

In Figure 8, we can see that the effect of N_B changes in shear velocity and stress on the wall is negligible.

In Figure 9, with increasing N_B, the slope of temperature change in the region close to the wall $\eta \cong 0$ increases, and this will increase the heat transfer in this region because this slope has a direct effect on the Nusselt number.

As shown in Figure 10, the mass transfer of nanoparticles to the outside of the boundary layer decreases with increasing the N_B; however, the intensity of the changes gradually becomes minimal. Note that the difference between $N_B = 0.1$ and $N_B = 0.2$ curves is high; however, with increasing N_B to 0.4, these differences are minimal.

In Figure 11, as N_B increases, the slope of the change curve becomes smooth in the middle distances between the wall and the end of the boundary layer, as in small amounts of N_B, this curve changes abruptly, but with increasing N_B, these sudden changes gradually decrease, and the curve becomes smooth.

In Figure 12, more Brownian motions near the wall, which is due to the greater mass of nanoparticles near the wall and causes severe temperature changes in this region. However, by gradually moving away from the wall, the nanoparticle mass decreases. As a result, the gravitational forces decrease, and the slope of temperature changes decreases. In other words, with increasing N_B, the slope of velocity changes near the wall becomes steeper. Increasing velocities near the wall, the convective heat transfer increases. In contrast, the thickness of the velocity boundary layer changes slightly.

As shown in Figure 13, contrary to N_B, the effect of N_T on the curves f' and f'' is negligible.

In Figure 14, we show temperature curves for N_T changes. As the N_T increases, the temperature gradient increases to half the thickness of the thermal boundary layer and then decreases again. Contrary to N_B, which had a decreasing trend for larger N_B values, the difference in the curve remains almost constant. With increasing the N_T number from 0.05 to 0.10, the differences in the temperature curves are almost the same as that of the N_T number from 0.20 to 0.25.

In Figure 15, at distances away from the wall, with increasing N_T, we see sudden changes in the nanoparticles mass. Mass transfer of nanoparticles along the boundary layer thickness and the slope of the changes at $N_T = 0.05$ is smooth and without sharp changes. As N_T increases, the slope of the curves gradually becomes steeper so that the inflection point of the curve is around $\eta = 0.7$.

Increasing N_T to 0.25, the slope of the curves is reversed and takes negative values. At the same time, the changes of the curves with increasing N_T are continuously increasing. It is noteworthy that the trend changes ϕ near the wall with increasing N_T inversely that it is far away. Hence, the slope of the curve decreases with increasing N_T and then increases in the middle along the wall to the edge of the boundary layer.

In Figure 16, the slope changes of θ' and ϕ' curves versus distance from the wall, η, are shown for various N_T. The slope of the curve ϕ' increases with increasing the N_T number in the regions close to the wall to the middle of the boundary layer. From this point to the edge of the boundary layer, with increasing N_T, the slope of the ϕ' curve decreases and then increases. Contrary, the slope of the θ' curve for each N_T is almost constant.

In Figure 17, the changes in temperature, nanoparticle mass transfer, and velocity curves along the plane for N_T changes from 0.05 to 0.25 are shown. We can see a slight difference in the f' curves compared to the more considerable difference in the θ and ϕ curves. As a result, N_T change has a negligible effect on u velocity.

We can see in Figure 18, that as the ratio of the buoyancy force to Reynolds square increases, the flow velocity is severely affected. Therefore, the effect of λ on changes in velocity and shear stress on the wall is more significant than N_B or N_T.

In Figure 19, with a change in λ, the rate of temperature gradient and the heat transfer changes slightly, and this trend gradually decreases with increasing λ. At the same time, the shear stress on the wall and the velocity inside the boundary layer are strongly affected. However, these velocity changes cause a slight change in temperature or nanoparticle mass transfer.

As shown in Figure 20, the changes ϕ, as well as the changes in its slope for λ changes, are minimal.

As shown in Figure 21, the effect λ on the slope curves of temperature and nanoparticle mass is much less than that of N_B and N_T.

In Figure 22, we show the number of significant changes in f' compared to small changes in θ and ϕ with an increasing value of λ.

Here, in Figures 23 and 24, assuming that the values of θ and ϕ are constant on the wall. The changes of f', f'', θ, and ϕ variables at different values ξ versus the thickness of the boundary layer are shown. As can be seen, the variables are very sensitive to the change of ξ. Of course, we expected such changes since convective heat transfer plays a significant role in the problem (λ = 1). The changes are intensified by increasing η in small ξ. In Figure 23, the overall shape of u velocity and shear stress profiles tend to be that of forced convection. The boundary layer thickness decreases from about 4.0 to 1.9 with increasing ξ. As shown in Figure 24, the thickness of the thermal and the nanoparticle mass boundary layers increase from about 1.3 to 3.6 and 1.6 to 4.0, respectively.

Figure 25 shows the changes of the θ and ϕ in the case they are changing on the longitudinal axis $\xi, \theta = a\xi, \phi = a\xi$, $a = 1$. As expected, when θ decreases with decreasing ξ, the effect of natural convection heat transfer increases; however, the f' profile becomes more similar to that of natural convection. In sum, the N_T change is due to a change in $(T - T_\infty)/T_\infty$, so it directly increases the slope intensity of the temperature curve, and this changes the balance between the thermophoresis and frictional forces (Eq. 19). Here, in addition to changes in temperature curves, we also see a change in mass nanoparticle transfer. This change is so severe that it creates a point of deflection in the curve of mass nanoparticle transfer. Also, the fluid velocity, which is affected by the buoyancy force, is expected to change significantly as the temperature changes. However, contrary to expectations, these changes are negligible (Eq. 19).

$$\frac{\partial\left(u^2 - U_\infty{}^2\right)}{2\partial x} + \left(u - U_\infty\right)\frac{\nu}{k} + \left(u^2 - U_\infty{}^2\right)\frac{\Gamma}{\sqrt{k}} \approx \nu\frac{\partial^2 u}{\partial y^2} + \left[\left(1-\varphi_\infty\right)\beta_T\left(T - T_\infty\right) - \left(\frac{\rho_p}{\rho_f} - 1\right)\left(\varphi - \varphi_\infty\right)\right]g \tag{19}$$

On the other hand, increasing the buoyancy force relative to the inertial force, λ, has a direct effect on the f' and f'' curves while affecting θ and ϕ slightly. In contrast, the change in nanoparticle mass transfer affects all variables f', f'' and θ, while the change θ is significant.

6. Conclusion:

In the present paper, we concern with the mixed convection heat transfer and fluid flow of a nanofluid in a saturated porous medium in a stagnation point region. At the same time, the longitudinal coordinate (the x-axis) effects are taken into account. In previous papers in the literature, the longitudinal coordinate effects are assumed to be negligible. Whereas, in the presence of suction/blowing, or if the temperature of the lateral mass flux depends on the x-coordinate along the substrate plate, the similar assumption of profile in the x-coordinate along is not accepted. The non-similar solution of a saturated nanofluid flow, heat, and mass transfer under dual effects of stagnation flow and natural convection heat transfer in a porous medium is presented in this paper. The dimensionless x-axis coordinate ξ is considered as the secondary non-similar variable, so the effects of forced convection, where the plate temperature depends on the longitudinal x-axis, can be appropriately investigated. We use the 45 Runge–Kutta methods with the shooting approach to solving differential equations. The effects of changes in the variables of thermal motion, Brownian motion, and buoyancy forces have been studied by considering the longitudinal effects of the x-axis, which is the innovation of the article.

The results show that:

1- The similarity solution has not sufficient accuracy in this problem.
2- In solving the equations of motion, we show that the minimum accuracy for the first-order non-similar solution in regions ξ <0.25, very close to the stagnation point, is 96%, while in regions greater than $\xi \geq 0.5$ it increases to 98%.
3- The effect of N_T changes in longitudinal velocity, and shear stress are almost negligible.
4- N_B changes also have little effect on them.

5- Increasing the natural convection has a significant effect on the longitudinal velocity profile, particularly in reducing the thickness of the velocity boundary layer.
6- Increasing λ also significantly reduces shear stress on the wall.
7- However, increasing λ does not increase heat transfer since the forced convection reduces.
8- Increasing the thermophoresis and Brownian motion increases the heat transfer within the thermal boundary layer, but the higher the amount, the less the effect.
9- As the point of stagnation approaches, regardless of whether the temperature and the number of nanoparticles on the bottom plate are constant or variable, the rate of change in the longitudinal velocity, shear stress, temperature profile, and mass distribution profile of the nanoparticle is severely affected. Interestingly, the thickness of the velocity boundary layer decreases rapidly, up to 38%, as it moves away from the point of stagnation.
10- Also, the shear stress becomes negative at some points close to the point of stagnation, which is a sign of backflow in the presence of convective heat transfer in stagnation flow.

References:

1. Kalogirou, S.A. "Solar thermal collectors and applications", Progress in Energy and Combustion Science, **30**(3), pp. 231-295 (2004).
2. Abbasi_Shavazi, E., Chen, J., Coventry, j., et al. "Progress in heat transfer research for high-temperature solar thermal applications", Applied Thermal Engineering, **184**, pp. 116137 (2021).
3. Razvan Budua, A., Lazaro Pavela, G. and Eugeniu Morarua, D. "Heat and mass transfer aspects in nuclear power generation", Energy Procedia, **112**, pp. 571–578 (2017).
4. Parizad Benam , B., Khalili Sadaghiani, A., Yağcı, V., et al. "Review on high heat flux flow boiling of refrigerants and water for electronics cooling", International journal of heat and mass transfer, **180**, pp. 121787 (2021).
5. Zhang, Zh., Wang, X. and Yan, Y. "A review of the state-of-the-art in electronic cooling", e-Prime - Advances in Electrical Engineering, Electronics and Energy, **1**, pp. 100009 (2021).
6. Weidman, P.D. and Mahalingam, S. "Axisymmetric Stagnation-Point Flow Impinging on a Transversely Oscillating Plate with Suction", Journal of Engineering Mathematics, **31**, pp. 305-318 (1997).
7. Shokrgozar Abbasi, A. and Rahimi, A.B. "Three-dimensional stagnation-point flow and heat transfer on a flat plate with transpiration", Journal of Thermophysics and Heat Transfer, **23**(3), pp. 513-521 (2009).
8. Shokrgozar Abbasi, A. and Rahimi, A.B. "Non-axisymmetric three-dimensional stagnation-point flow and heat transfer on a flat plate", ASME. J. Fluids Eng., **131**(7), pp. 074501.1–074501.5 (2009).
9. Shokrgozar Abbasi, A. and Rahimi, A.B. "Investigation of Two-dimensional unsteady stagnation point-flow and heat transfer impinging on an accelerated flat plate", Journal of Heat Transfer, **134**, pp. 064501-5 (2012).
10. Shokrgozar Abbasi, A., Rahimi, A.B. and Mozayyeni, H. "Investigation of three-dimensional axisymmetric unsteady stagnation point-flow and heat transfer impinging on an accelerated flat plate", Journal of Applied Fluid Mechanics, **9**, pp. 451-461 (2016).
11. Rangel, R.H. and Bian, X. "The inviscid stagnation-flow solidification problem", International Journal of Heat and Mass Transfer, **39**(8), pp. 1591-1602 (1994).
12. Shokrgozar Abbasi, A. and Rahimi, A.B. "Solidification of Two-Dimensional Viscous, Incompressible Stagnation Flow", Journal of Heat Transfer. **135**, pp. 072301-072308 (2013).
13. Shokrgozar Abbasi, A. "Three-Dimensional Axisymmetric Solidification of a Viscous Incompressible Flow in the Stagnation Point Region", Journal of Applied Fluid Mechanics, **10**(1), pp. 413-420 (2017).
14. Shokrgozar Abbasi, A. and M. Ghayeni, "Water Vapor Solidification of Saturated Air in Two-Dimensional Stagnation Flow", Scientia Iranica, **27**(2), pp. 693-703 (2020).
15. Yih, K.A. "Heat source/sink effect on MHD mixed convection in stagnation flow on a vertical permeable plate in porous media", International Communications in Heat and Mass Transfer, **25**, pp. 427–442 (1988).
16. Choi, S.U.S. "Nanofluids: From Vision to Reality Through Research." ASME. J. Heat Transfer, **131**(3), pp. 033106 (2009).
17. Timofeeva, E.V., Yu, W., France, D.M., et al. "Nanofluids for heat transfer: an engineering approach", Nanoscale Res Lett, **6**, pp. 182 (2011).
18. Adnan Khan, U., Ahmed, S.T. Mohyud-Din, M.D., et al. "A novel analysis of heat transfer in the nanofluid composed by nanodimaond and silver nanomaterials:

numerical investigation.", Sci Rep, **12**, pp. 1284 (2022).
19. Okonkwo, E.C., Wole-Osho, I., Almanassra, I.W., et al. "An updated review of nanofluids in various heat transfer devices", J Therm Anal Calorim, **145**, pp. 2817–2872 (2021).
20. Cheng, p. "Combined free and forced convection flow about inclined surfaces in porous media", International Journal of Heat and Mass Transfer, **20**, pp. 807–814 (1977).
21. Nazar, R., Amin, N. and Pop, I. "Unsteady mixed convection boundary layer flow near the stagnation point on a vertical surface in a porous medium", International Journal of Heat and Mass Transfer, **47**, pp. 2681–2688 (2004).
22. Merrill, K. Beauchesne, M., Previte, J., et al. "Final steady flow near a stagnation point on a vertical surface in a porous medium", International Journal of Heat and Mass Transfer, **49**, pp. 4681–4686 (2006).
23. Ishak, A., Nazar, R., Arifin, N.M., et al. "Dual solutions in mixed convection flow near a stagnation point on a vertical porous plate", International Journal of Thermal Sciences, **47**(4), pp. 417-422 (2008).
24. Subhashini, S.V., Sumathi, R. and Momoniat, E. "Dual solutions of a mixed convection flow near the stagnation point region over an exponentially stretching/shrinking sheet in nanofluids", Meccanica, **49**, pp. 2467–2478 (2014).
25. Sparrow, E.M. and Yu, H.S. "Local Non-Similarity Thermal Boundary-Layer Solutions", ASME. J. Heat Transfer, **71**, pp. 328-334 (1970).
26. Sparrow, E.M., Quack, H. and Boerner, C.J. "Local Nonsimilarity Boundary-Layer Solutions", AIAA Journal, **8**(11), pp. 1936-1942 (1970).
27. Minkowycz, W.J. and Cheng, p. "local non-similar solutions for free convective flow with uniform lateral mass flux in a porous medium", Letters in heat and mass transfer, **9**(3), pp. 159-168 (1982).
28. Jafarimoghaddam, A. "Numerical Analysis of the Nanofluids Flow Near the Stagnation Point over a Permeable Stretching/Shrinking Wall: A New Modeling", Arabian Journal for Science and Engineering, **45**, pp. 1001–1015 (2020).
29. Roşca, A.V., Roşca, N.C. and Pop, I. "Mixed convection stagnation point flow of a hybrid nanofluid past a vertical flat plate with a second order velocity model", International Journal of Numerical Methods for Heat and Fluid Flow, **31**(1), pp. 75-91 (2020).
30. Ferdows, M. Nabwey, H.A. Rashad, A., et al. "Boundary layer flow of a nanofluid past a horizontal flat plate in a Darcy porous medium: A Lie group approach", Proceedings of the Institution of Mechanical Engineers, Part C: Journal of Mechanical Engineering Science, **234**(8), pp. 1545-1553 (2020).
31. Ramachandran, N., Chen, T.S. and Armaly, B.F. "Mixed Convection in Stagnation Flows Adjacent to Vertical Surfaces", Journal of Heat Transfer, **110**, pp. 373-377 (1988).
32. Duwairi, H.M., Damseh, R.A. and Tashtoush, B. "Transient Mixed Convection along a Vertical Plate Embedded in Porous Media with Internal Heat Generation and Oscillating Temperature", Chemical Engineering Communications, **194**, pp. 1516–1530 (2007).
33. Ishak, A., Nazar, R. and Pop, I. "Dual solutions in mixed convection flow near a stagnation point on a vertical surface in a porous medium", International Journal of Heat and Mass Transfer, **51**, pp. 1150–1155 (2008).
34. Srinivasacharya, D. and Surender, O. "Non-similar solution for natural convective boundary layer flow of a nanofluid past a vertical plate embedded in a doubly stratified porous medium", International Journal of Heat and Mass Transfer, **71**, pp. 431–438 (2014).
35. Abdullah, A., Ibrahim, F. and Chamkha, A. "Non-similar solution of unsteady mixed convection flow near the stagnation point of a heated vertical plate in a porous medium saturated with a nanofluid", Journal of porous media , **21**(4), pp. 363–388 (2018).
36. Ferdows, M. and Alzahrani, F. "Dual solutions of nanaofluid forced convective flow with heat transfer and porous media past a moving surface", Physica A: Statistical Mechanics and its Applications", **551**, pp. 124075 (2020). DOI: 10.1016/j.physa.2019.124075
37. Waini, I., Ishak, A. and Pop, I. "Hybrid nanofluid flow towards a stagnation point on a stretching/shrinking cylinder", Sci Rep. **10**, 9296 (2020). DOI: 10.1038/s41598-020-66126-2.
38. Khan, U., Zaib, A. and Ishak, A. "Non-similarity solutions of radiative stagnation point flow of a hybrid nanofluid through a yawed cylinder with mixed convection", Alexandria Engineering Journal, **60**(6), pp. 5297-5309 (2021).
39. Yih, K.A. "Heat source/sink effect on MHD mixed convection in stagnation flow on a vertical permeable plate in porous media, International Communications in Heat and Mass Transfer, **25**, pp. 427–442 (1988).
40. Rashad, A.M, Waqar, A.Kh., EL-Kabeir, A.M.M., et al. "Mixed Convective Flow of Micropolar Nanofluid

across a Horizontal Cylinder in Saturated Porous Medium", Applied Science, **9**, pp. 5241 (2019).

41. Hussein, A.K.M, Hamzah, H.K., Ali, F.H., et al. "Mixed convection in a trapezoidal enclosure filled with two layers of nanofluid and porous media with a rotating circular cylinder and a sinusoidal bottom wall, Journal of Thermal Analysis and Calorimetry, **141**(2), (2019). DOI:10.1007/s10973-019-08963-6.
42. Uddin, M.J., Khan, W.A., Anwar Bég, O., et al. "Non-Similar Solution of G-jitter Induced Unsteady Magnetohydrodynamic Radiative Slip Flow of Nanofluid", Applied Science, **10**(4), pp. 1420 (2020). DOI.org/10.3390/app10041420
43. Ramachandra Prasad, V., Abdulgaffar, S. and Rushi Kuma, B. "Non-Similar Comutational Solutions for Double-Diffusive MHD Transport Phenomena for Non-Newtonian Nanofluid From a Horizontal Circular Cylinder", Nonlinear Engineering, **8**(1), pp. 470-485 (2018). DOI.org/10.1515/nleng-2018-0035
44. Al-Farhany, Kh. and Abdulsahib, A.Dh. "Study of mixed convection in two layers of saturated porous medium and nanofluid with rotating circular cylinder", Progress in Nuclear Energy, **135**, pp. 103723 (2021). DOI.org/10.1016/j.pnucene.2021.103723.
45. Nabwey, H.A., EL-Kabeir, S.M.M., Rashad, A.M., et al. "Gyrotactic microorganisms mixed convection flow of nanofluid over a vertically surfaced saturated porous media", Alexandria Engineering Journal, **61**(3), pp. 1804-1822 (2022).

Brief technical biography:

Ali Shokrgozar Abbasi received his PhD degree from the Department of Mechanical Engineering, Ferdowsi University of Mashhad, Iran. He is Assistant professor Payame Noor University, Iran. His numerous researches articles in the field of heat transfer and fluid mechanics have been published in the reputable international journals.

No.	Figure captions
Fig. 1	Figure 1: schematic diagram of the problem (S.P.: Stagnation Point)
Fig. 2	Figure 2: u velocity variations along η, $N_B, N_T, \lambda = 1$, $\xi = 0.25,\ 0.33,\ 0.5,\ 0.75,\ 1.0$, $\theta_{wall} = \phi_{wall} = 1$
Fig. 3	Figure 3: u velocity variations along η, $N_B, N_T, \lambda = 1$, $\xi = 0.25,\ 0.5,\ 0.75,\ 1.0$, $\theta_{wall} = \phi_{wall} = \xi^{n=1}$
Fig. 4	Figure 4: temperature variations versus η, $N_B, N_T, \lambda = 1$, $\xi = 0.25,\ 0.33,\ 0.5,\ 0.75,\ 1.0$, $\theta_{wall} = \phi_{wall} = Const.$
Fig. 5	Figure 5: temperature variations versus η, $N_B, N_T, \lambda = 1$, $\xi = 0.25,\ 0.33,\ 0.5,\ 0.75,\ 1.0$, $\theta_{wall} = \phi_{wall} = \xi^{n=1}$
Fig. 6	Figure 6: All variables and their derivatives respect to η, $N_B, N_T, \lambda, \xi = 1$
Fig. 7	Figure 7: All variables and their derivatives respect to ξ, $N_B, N_T, \lambda, \xi = 1$
Fig. 8	Figure 8: Velocity u, and shear stress variations along, $N_T, \lambda, \xi = 1$, $N_B = 0.1, 0.2, 0.3, 0.4$
Fig. 9	Figure 9: Temperature and its derivative variations along η $N_T, \lambda, \xi = 1$, $N_B = 0.1, 0.2, 0.3, 0.4$
Fig. 10	Figure 10: Nanoparticle mass and its derivative variations along η, $N_T, \lambda, \xi = 1$, $N_B = 0.1, 0.2, 0.3, 0.4$
Fig. 11	Figure 11: Derivatives of the temperature and Nanoparticle mass along η, $N_T, \lambda, \xi = 1$, $N_B = 0.1, 0.2, 0.3, 0.4$
Fig. 12	Figure 12: Temperature, Nanoparticle mass, and u velocity variations along η, $N_T, \lambda, \xi = 1$, $N_B = 0.1, 0.2, 0.3, 0.4$
Fig. 13	Figure 13: u velocity and shear stress variations along η, $N_B, \lambda, \xi = 1$, $N_T = 0.05, 0.1, 0.15, 0.2, 0.25$

Fig. 14	Figure 14: Temperature and its derivative variations along η, $N_B, \lambda, \xi = 1$, $N_T = 0.05, 0.1, 0.15, 0.2, 0.25$
Fig. 15	Figure 15: Nanoparticle mass and its derivative variations along η, $N_B, \lambda, \xi = 1$, $N_T = 0.05, 0.1, 0.15, 0.2, 0.25$
Fig. 16	Figure 16: Derivatives of Nanoparticle mass and Temperature variations along η, $N_B, \lambda, \xi = 1$, $N_T = 0.05, 0.1, 0.15, 0.2, 0.25$
Fig. 17	Figure 17: Temperature, Nanoparticle mass, and u velocity variations along η, $N_B, \lambda, \xi = 1$, $N_T = 0.05, 0.1, 0.15, 0.2, 0.25$
Fig. 18	Figure 18: u velocity and shear stress variations along η, $N_B, N_T, \xi = 1, \lambda = 1, 2, 3$
Fig. 19	Figure 19: Temperature and its derivative variations along η, $N_B, N_T, \xi = 1, \lambda = 1, 2, 3$
Fig. 20	Figure 20: Nanoparticle mass and its derivative variations along η, $N_B, N_T, \xi = 1, \lambda = 1, 2, 3$
Fig. 21	Figure 21: Derivatives of Nanoparticle mass and temperature variations along η, $N_B, N_T, \xi = 1, \lambda = 1, 2, 3$
Fig. 22	Figure 22: Temperature, Nanoparticle mass, and u velocity variations along η, $N_B, N_T, \xi = 1, \lambda = 1, 2, 3$
Fig. 23	Figure 23: u velocity and shear stress variations along η, $N_B, N_T, \lambda = 1$, $\xi = 1.0, 0.33, 0.25, 0.17, 0.1$, $\theta_{wall} = \phi_{wall} = Const.$
Fig. 24	Figure 24: Temperature and nanoparticle variations versus η, $N_B, N_T, \lambda = 1$, $\xi = 1.0, 0.33, 0.25, 0.17, 0.1$, $\theta_{wall} = \phi_{wall} = Const.$
Fig. 25	Figure 25: temperature, θ, and nanoparticle, ϕ, variations versus η, $N_B, N_T, \lambda = 1$, $\xi = 1.0, 0.75, 0.50, 0.25, 0.2$, $\theta = \xi, \phi = \xi$

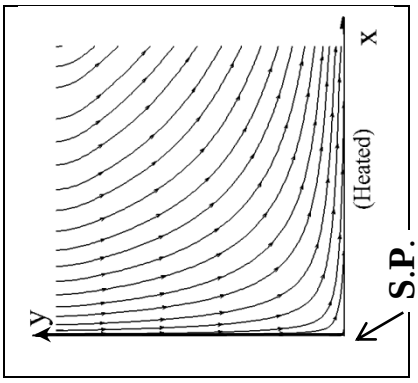

Figure 1: schematic diagram of the problem (S.P.: Stagnation Point)

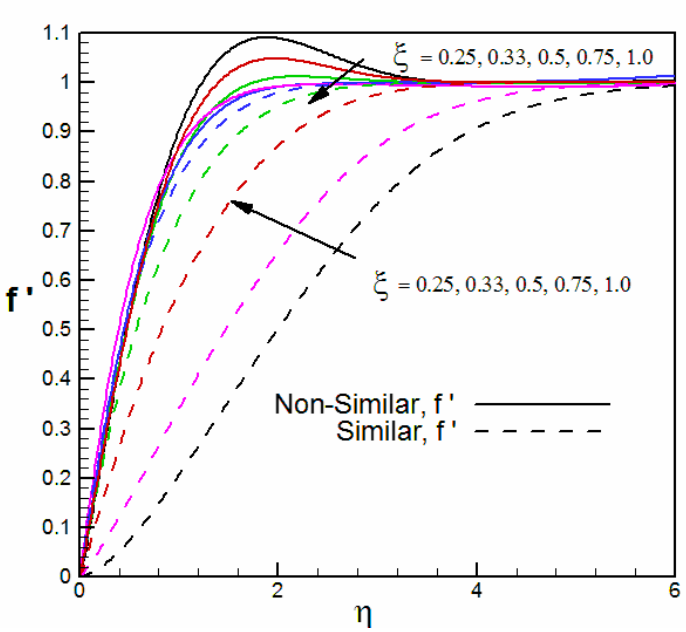

Figure 2: u velocity variations along η,

$N_B, N_T, \lambda=1$, $\xi=0.25,\ 0.33,\ 0.5,\ 0.75,\ 1.0$, $\theta_{wall}=\phi_{wall}=1$

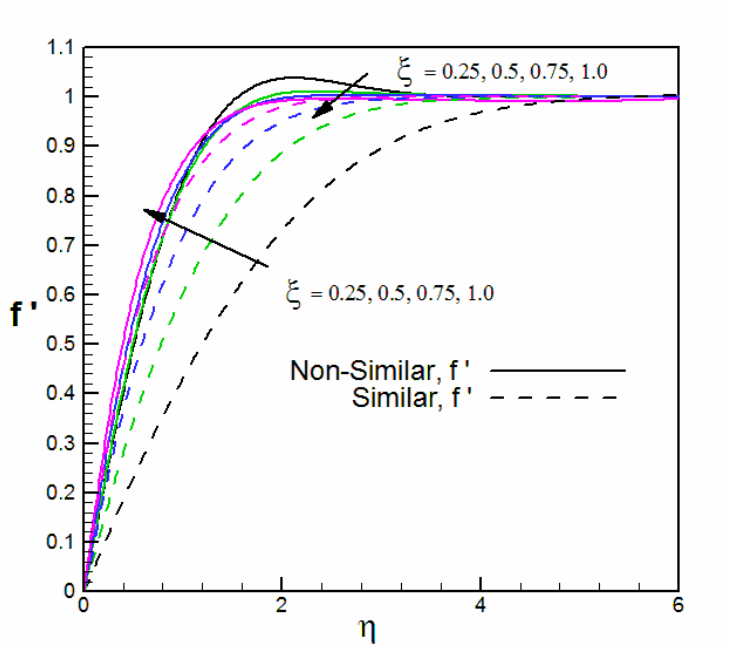

Figure 3: u velocity variations along η,

$N_B, N_T, \lambda = 1$, $\xi = 0.25,\ 0.5,\ 0.75,\ 1.0$, $\theta_{wall} = \phi_{wall} = \xi^{n=1}$

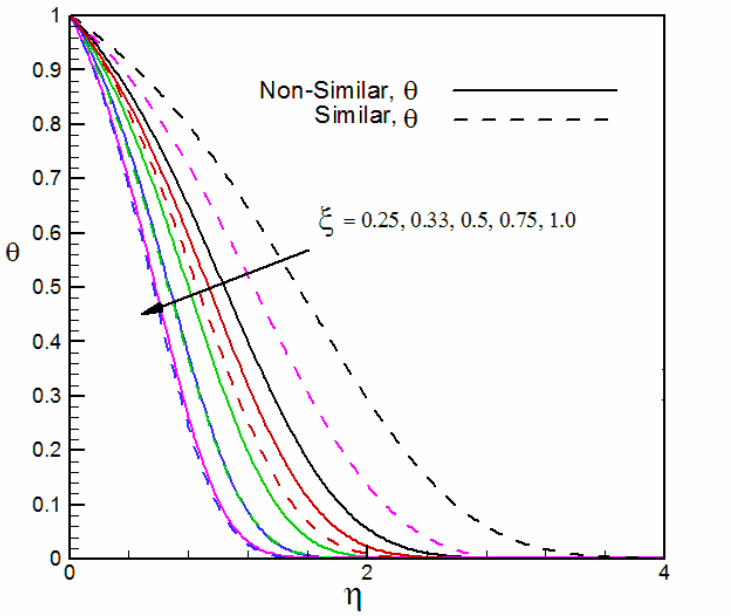

Figure 4: temperature variations versus η,

$N_B, N_T, \lambda = 1$, $\xi = 0.25,\ 0.33,\ 0.5,\ 0.75,\ 1.0$, $\theta_{wall} = \phi_{wall} = Constant$

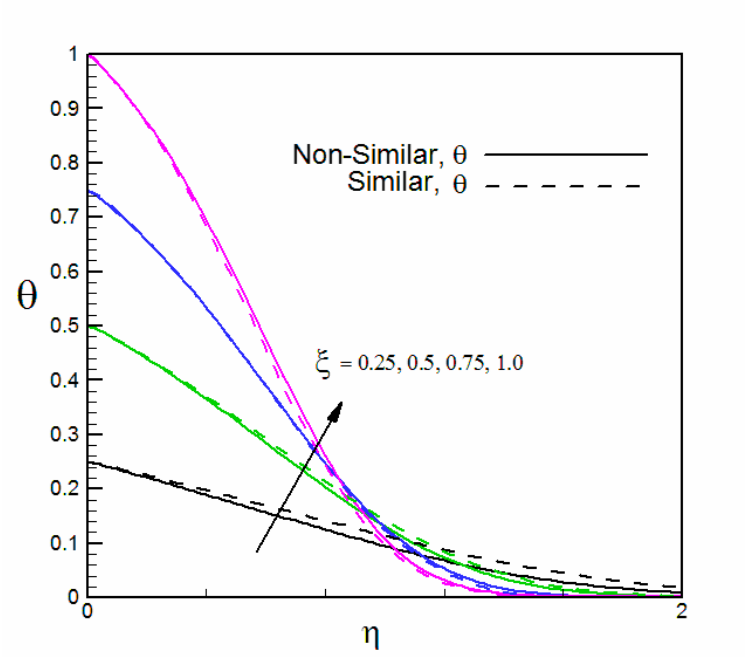

Figure 5: temperature variations versus η,

$N_B, N_T, \lambda=1$, $\xi=0.25,\ 0.33,\ 0.5,\ 0.75,\ 1.0$, $\theta_{wall}=\phi_{wall}=\xi^{n=1}$

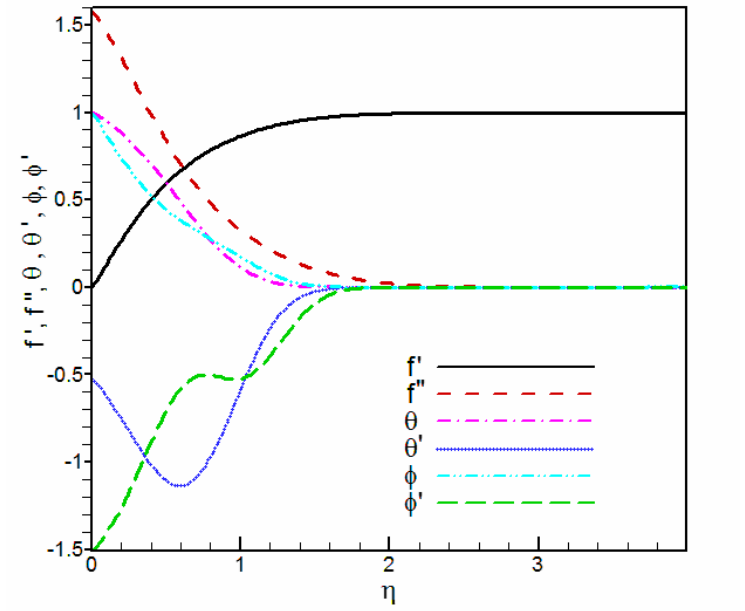

Figure 6: All variables and their derivatives respect to η,

$N_B, N_T, \lambda, \xi=1$

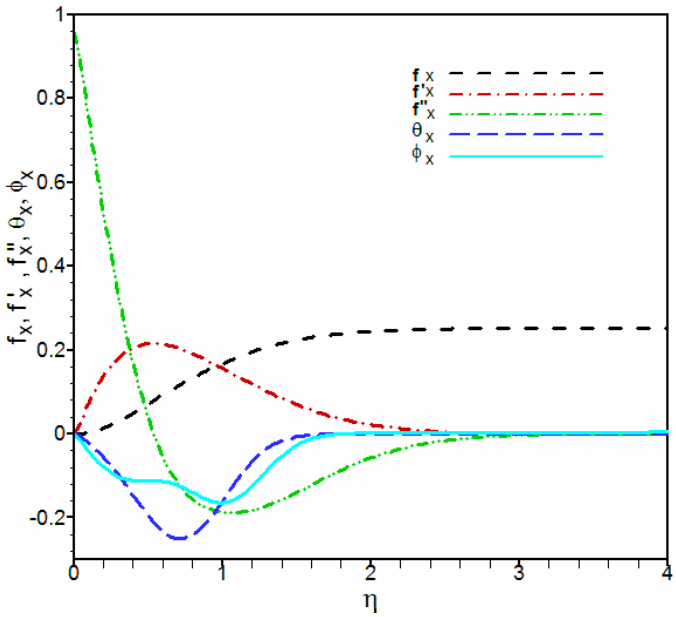

Figure 7: All variables and their derivatives respect to ξ, $N_B, N_T, \lambda, \xi = 1$

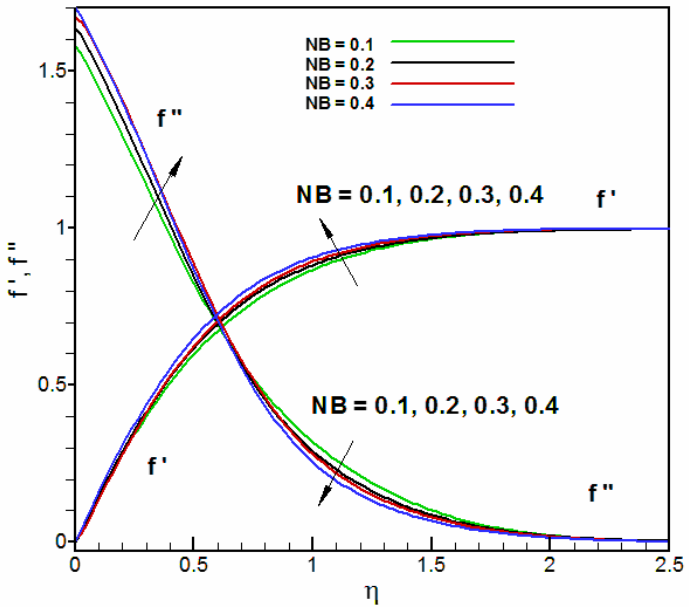

Figure 8: Velocity u, and shear stress variations along, $N_T, \lambda, \xi = 1$, $N_B = 0.1, 0.2, 0.3, 0.4$

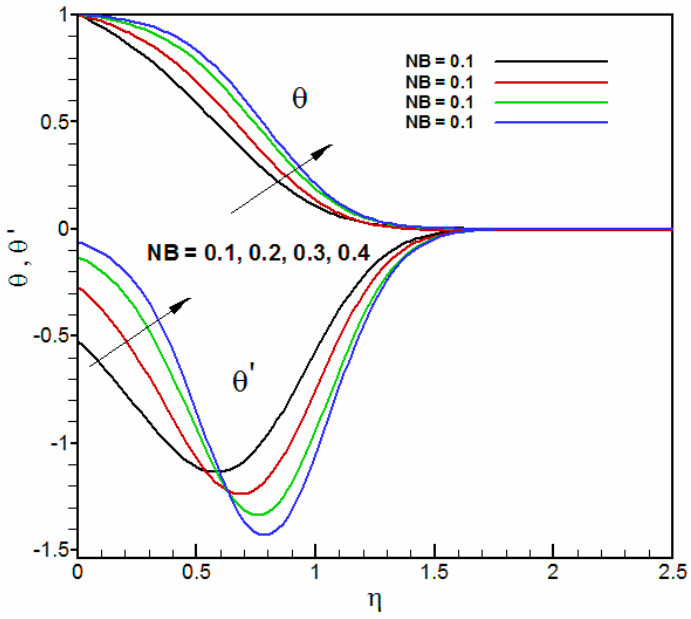

Figure 9: Temperature and its derivative variations along η

$N_T, \lambda, \xi = 1,\ N_B = 0.1, 0.2, 0.3, 0.4$

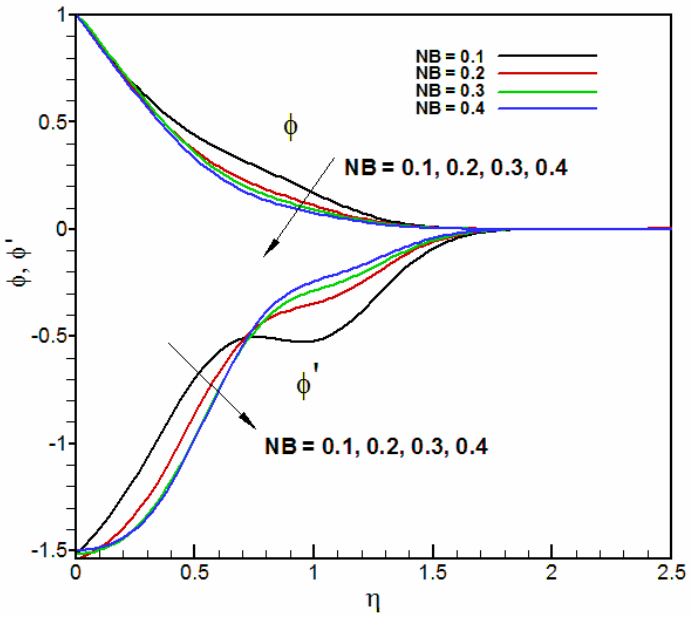

Figure 10: Nanoparticle mass and its derivative variations along η,

$N_T, \lambda, \xi = 1,\ N_B = 0.1, 0.2, 0.3, 0.4$

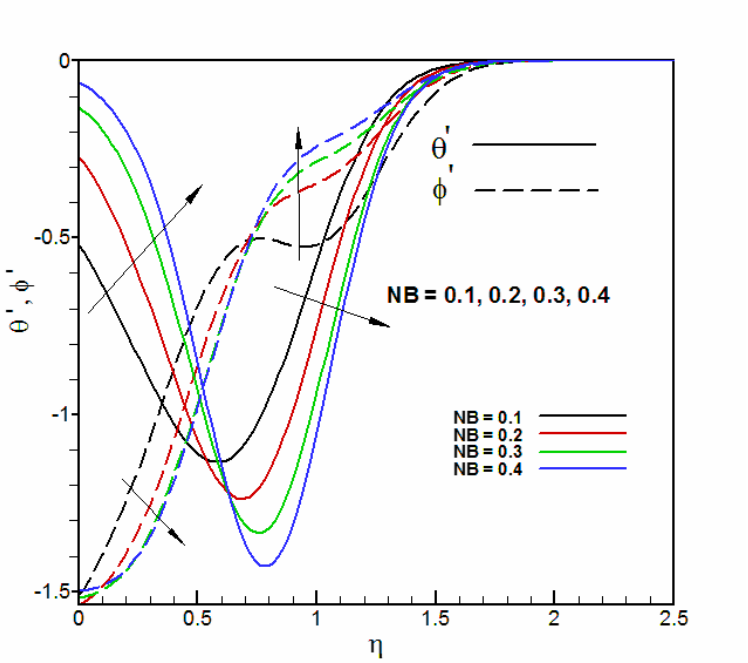

Figure 11: Derivatives of the temperature and Nanoparticle mass along η,

$N_T, \lambda, \xi = 1,\ N_B = 0.1, 0.2, 0.3, 0.4$

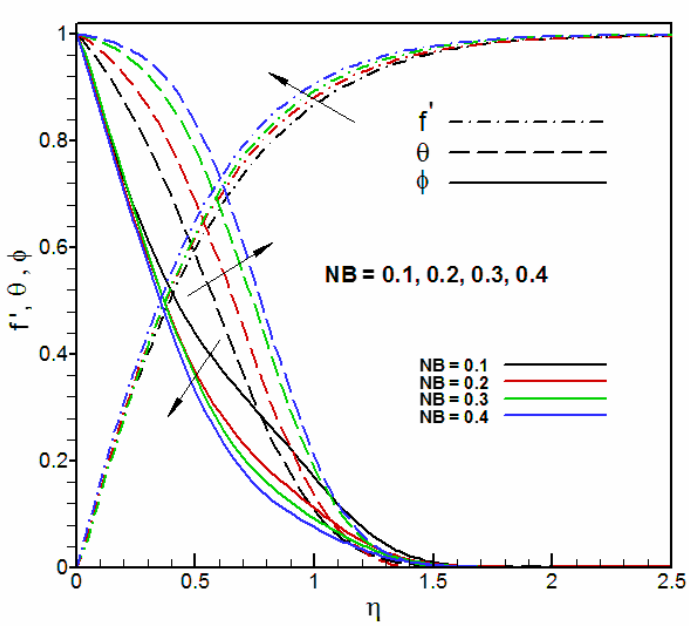

Figure 12: Temperature, Nanoparticle mass, and u velocity variations along η,

$N_T, \lambda, \xi = 1,\ N_B = 0.1, 0.2, 0.3, 0.4$

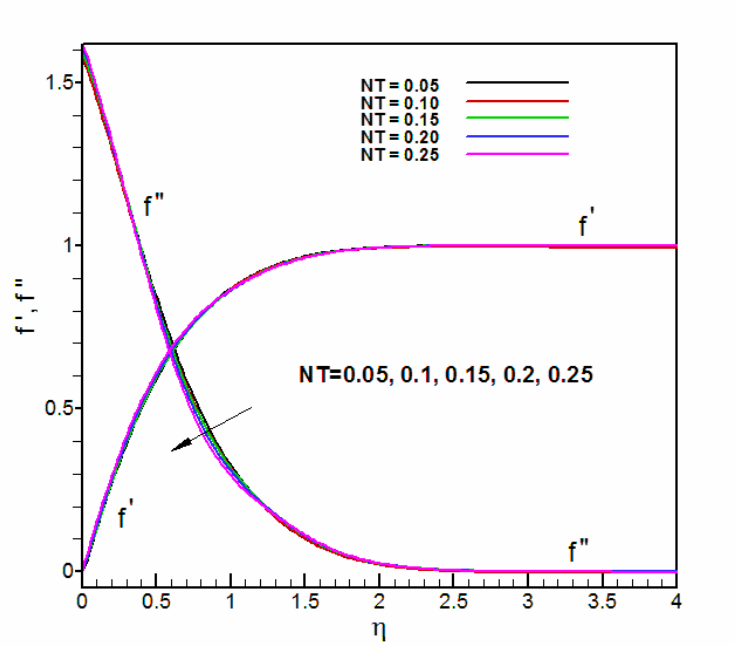

Figure 13: u velocity and shear stress variations along η,
$N_B, \lambda, \xi = 1$, $N_T = 0.05, 0.1, 0.15, 0.2, 0.25$

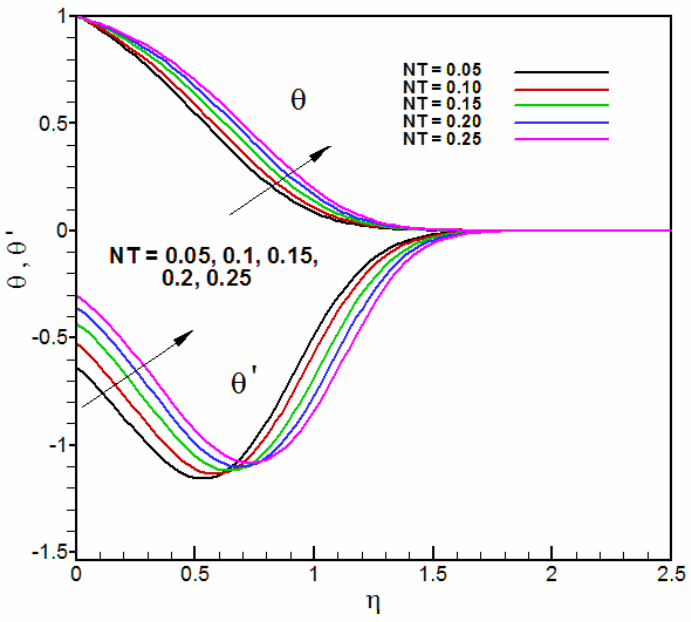

Figure 14: Temperature and its derivative variations along η,
$N_B, \lambda, \xi = 1$, $N_T = 0.05, 0.1, 0.15, 0.2, 0.25$

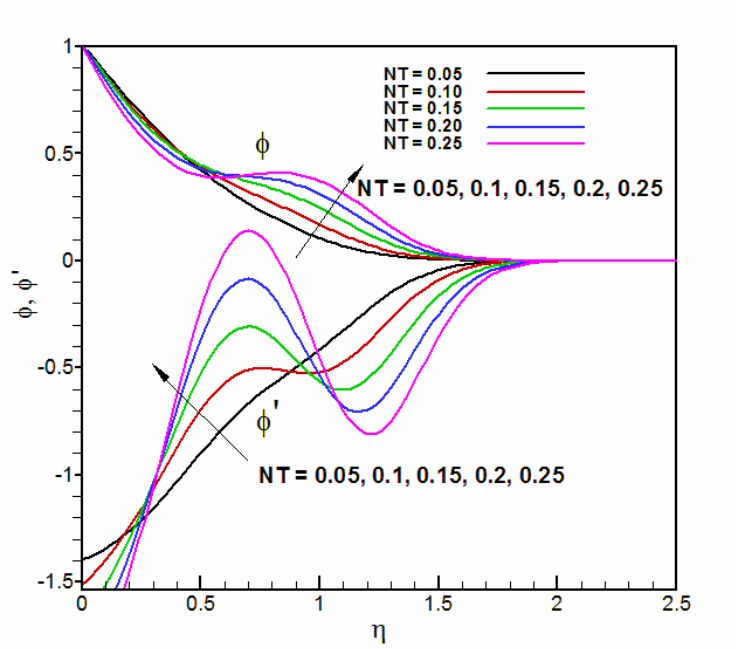

Figure 15: Nanoparticle mass and its derivative variations along η,
$N_B, \lambda, \xi = 1$, $N_T = 0.05, 0.1, 0.15, 0.2, 0.25$

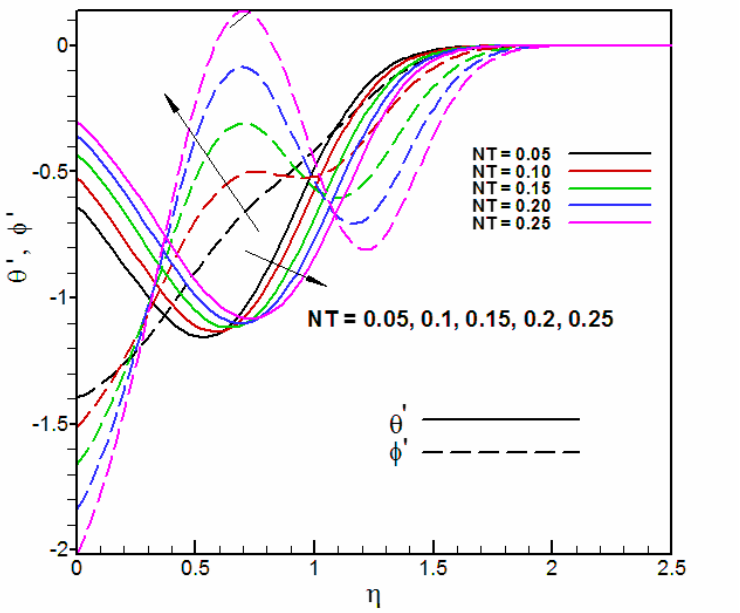

Figure 16: Derivatives of Nanoparticle mass and Temperature variations along η,
$N_B, \lambda, \xi = 1$, $N_T = 0.05, 0.1, 0.15, 0.2, 0.25$

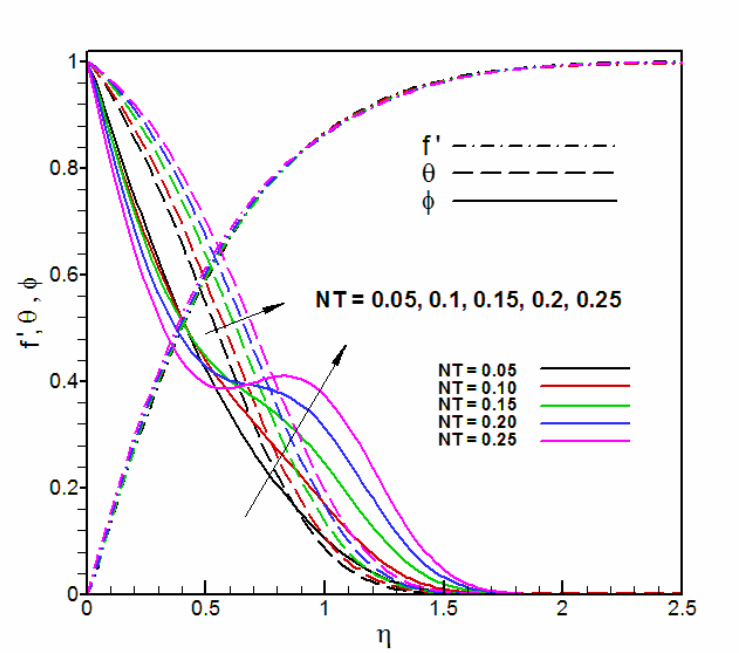

Figure 17: Temperature, Nanoparticle mass, and u velocity variations along η, $N_B, \lambda, \xi = 1$, $N_T = 0.05, 0.1, 0.15, 0.2, 0.25$

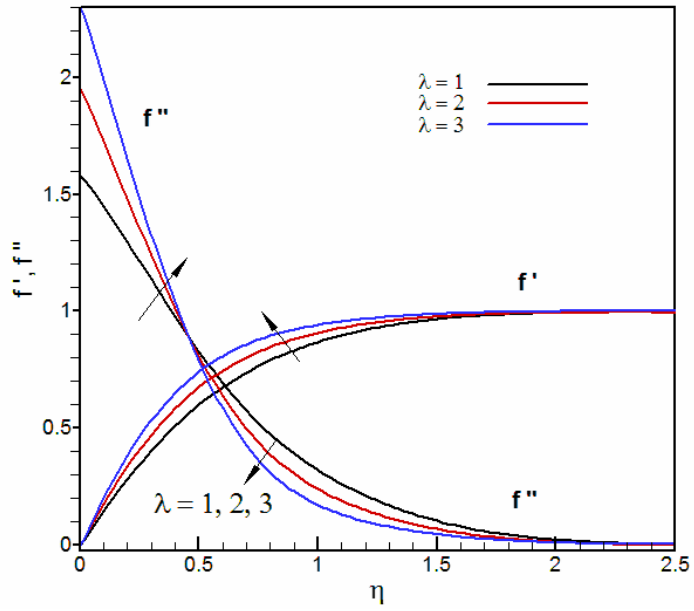

Figure 18: u velocity and shear stress variations along η, $N_B, N_T, \xi = 1$, $\lambda = 1, 2, 3$

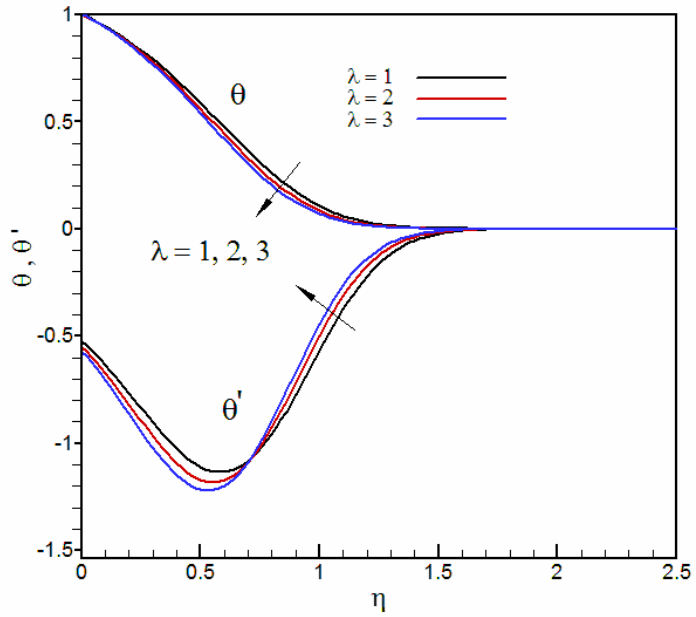

Figure 19: Temperature and its derivative variations along η, $N_B, N_T, \xi = 1,\ \lambda = 1, 2, 3$

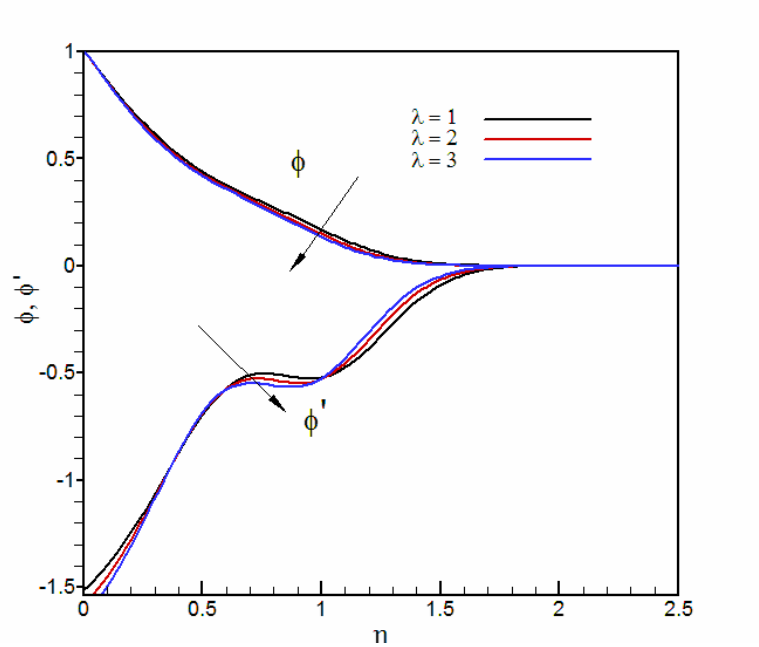

Figure 20: Nanoparticle mass and its derivative variations along η, $N_B, N_T, \xi = 1,\ \lambda = 1, 2, 3$

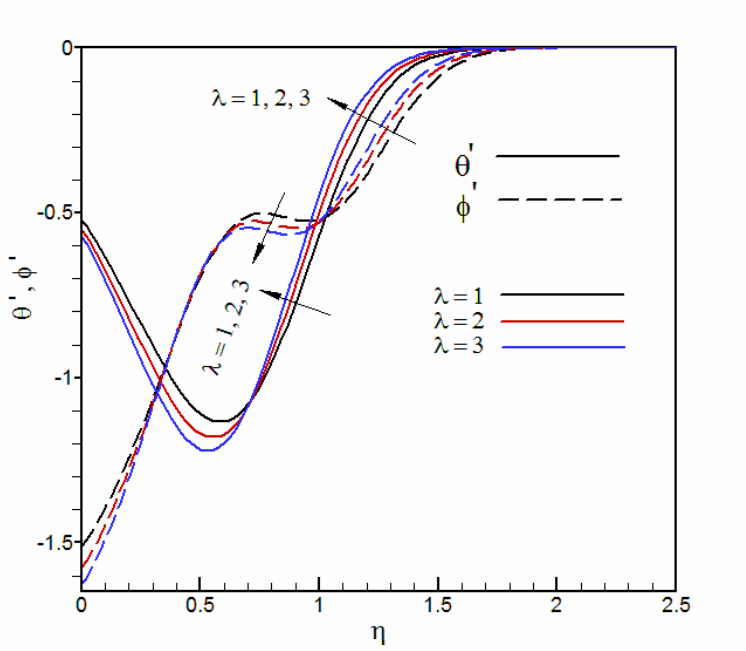

Figure 21: Derivatives of Nanoparticle mass and temperature variations along η, $N_B, N_T, \xi = 1,\ \lambda = 1, 2, 3$

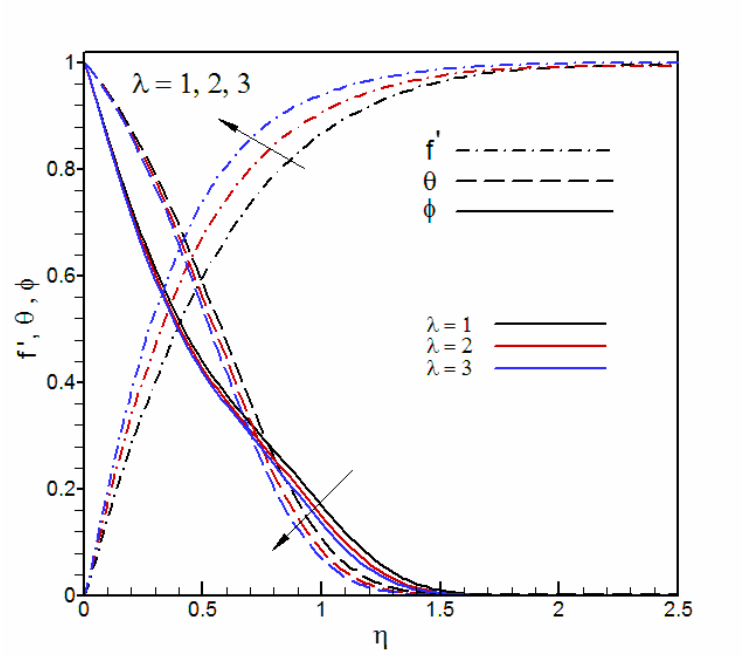

Figure 22: Temperature, Nanoparticle mass, and u velocity variations along η, $N_B, N_T, \xi = 1,\ \lambda = 1, 2, 3$

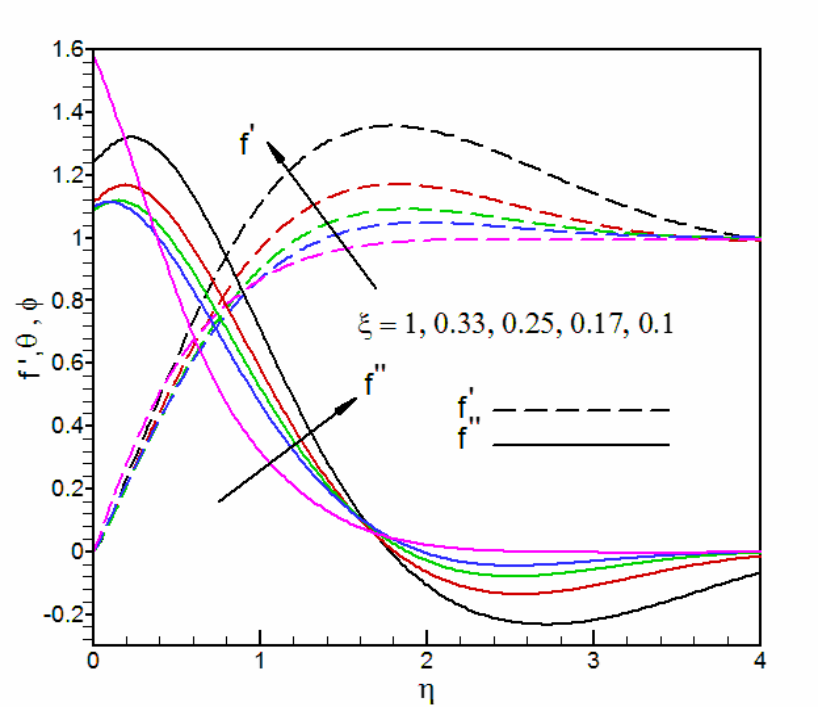

Figure 23: u velocity and shear stress variations along η,

$N_B, N_T, \lambda = 1$, $\xi = 1.0, 0.33, 0.25, 0.17, 0.1$, $\theta_{wall} = \phi_{wall} = Constant$

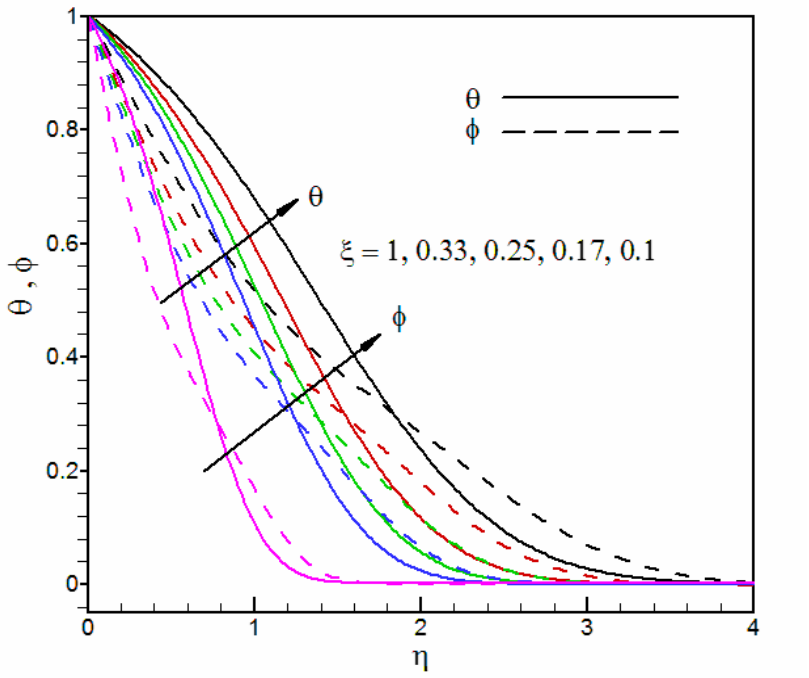

Figure 24: Temperature and nanoparticle variations versus η,

$N_B, N_T, \lambda = 1$, $\xi = 1.0, 0.33, 0.25, 0.17, 0.1$, $\theta_{wall} = \phi_{wall} = Constant$

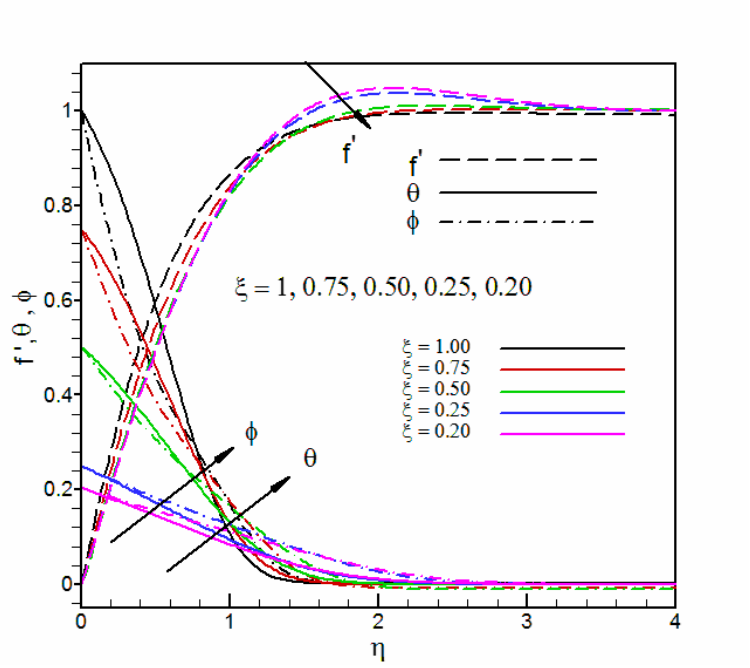

Figure 25: temperature, θ, and nanoparticle, ϕ, variations versus η, $N_B, N_T, \lambda = 1$， $\xi = 1.0, 0.75, 0.50, 0.25, 0.2$ ， $\theta = \xi$, $\phi = \xi$